

Design of a high-quality multi-terminal semiconductor switch

Juan Daniel Torres Luna

Design of a high-quality multi-terminal semiconductor switch

by

Juan Daniel Torres Luna

to obtain the degree of Master of Science
at the Delft University of Technology,
to be defended publicly on April 21st

Student number: 5213983
Project duration: August 31, 2021 – March 2, 2022
Thesis committee: Prof. Michael Wimmer, TU Delft, supervisor
Prof. Anton Akhmerov TU Delft, co-supervisor
Dr. Chun-Xiao Liu TU Delft, co-supervisor

Contents

1	Background	1
1.1	Introduction	1
1.2	Majorana bound states	2
1.3	Experimental platforms	3
1.3.1	Two dimensional electron gases	3
1.3.2	Electrostatic gates	4
1.4	Majorana bound states in a trijunction	4
2	Trijunction of Majorana nanowires	5
2.1	Quasi-one dimensional cavities	5
2.1.1	Size dependence	6
2.1.2	Resonant trapping	7
2.2	Two dimensional cavities	7
2.2.1	Size dependence	8
2.2.2	Angular dependence	9
2.2.3	Majorana sub bands	10
3	Gate defined triangular cavities	11
3.1	Gates configuration	11
3.2	Device 1	12
3.2.1	Nanowire channels	13
3.2.2	Background potential	13
3.2.3	Device operation	14
3.3	Device 2	14
3.3.1	Nanowire channels	15
3.3.2	Potential background	16
3.3.3	Device operation	16
3.4	Devices comparison	16
4	Conclusions	18
	Bibliography	19

1

Background

1.1. Introduction

MBS appear as the zero-energy modes of a hybrid quasi-one dimensional system that combines a strong-spin orbit semiconductor with proximity induced superconductivity. Semiconducting nanowires and two-dimensional electron gases (2DEG) are candidates for creating such devices, yet no evidence of such excitations has been found. Nevertheless, the existence of MBS would allow us to design new qubits that are resilient to noise in contrast to current devices.

While coupling a single MBS pair can be done using a quantum dot, selective coupling of multiple pairs remains a challenge. In the presence of multiple pairs, coupling MBS from different fermions induces a non-trivial evolution of the ground state that supports quantum gate operation. Coupling of a pair of MBS in a S-N-S junction has been extensively studied, and the fractional Josephson effect has been found as a signature of MBS present in such system. On the other hand, coupling multiple MBS pairs remains a challenge given the constraints on the nanowires alignment and separation.

The simplest system where multiple MBS can couple non-trivially is in a trijunction geometry. *In this thesis we propose a semiconducting cavity connected to three Majorana nanowires that allows for an all-electric controlled interaction between all pairs of MBS.*

Initially, the role of geometry is investigated by simulating several cavity geometries and extracting the MBS coupling in the strong coupling regime. It is found that different cavity levels mediate differently the coupling of different MBS pairs. We found that there is an angle for a triangular cavity that induces a maximum coupling between the far MBS pairs. *Several cavity geometries are analysed, and a triangular cavity with varying angle is found to have the largest coupling for all pairs.*

Finally, a realistic model is studied via electrostatic simulations of the triangular cavity with optimal configuration defined on a 2DEG. The non-local nature of the gates makes the nanowire positions crucial in order to recover the effects found for the purely geometric case. The role of each set of gates and the range of voltages used to operate the device are discussed. *The electrostatics effects of the gate-defined triangular cavity are analysed and the operational point is described.*

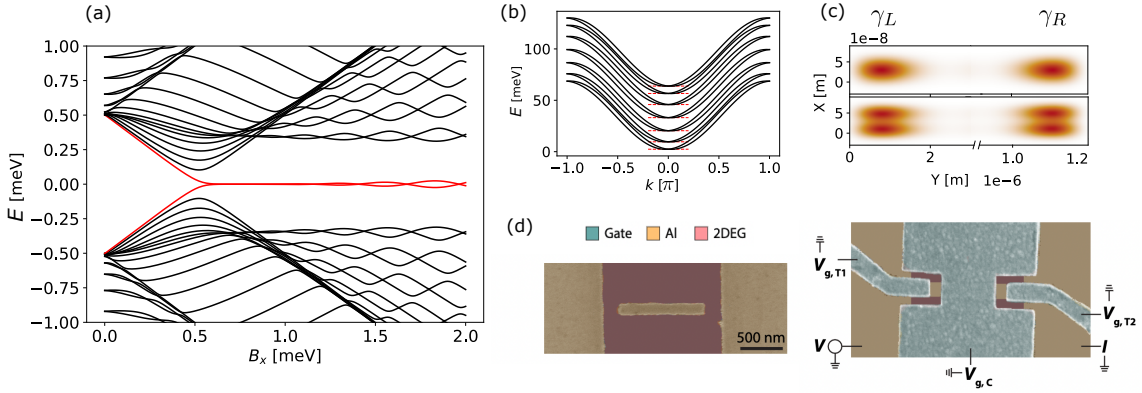


Figure 1.1: Simulations of a Majorana nanowire as described in Eq. (1.4). The following parameters will be used in all simulations: $\Delta = 0.5[\text{meV}]$, $\alpha = 0.3[\text{eV A}]$, and $m^* = 0.023m_e$. Each simulated nanowire has length $L = 120 * a$ and width $W = 7 * a$ where $a = 10[\text{nm}]$ is the lattice constant size. (a) Topological phase transition as a function of Zeeman field B_x . Lowest mode (red) sticks to zero after crossing the critical field. (b) Transverse bands along the translational invariant direction with $\Delta = 0$. The chemical potential is tuned to the bottom of each band (red dashed lines) to create Majoranas. (c) Majorana wavefunctions for the lowest two bands. (d) SEM image of a superconducting island with stripe shape taken from Ref. [3]. Right panel shows system after deposition of metallic gates.

1.2. Majorana bound states

MBS populate the non-local degenerate ground state of a topological superconductor. Under the appropriate conditions, a spinless one-dimensional p -wave superconductor contains two zero-energy excitations that are exponentially localised at the edges of the system. Together, these two zero-energy modes encode a single fermionic mode that can be empty or occupied,

$$f = \frac{\gamma_L + i\gamma_R}{\sqrt{2}}, \quad f^\dagger = \frac{\gamma_L - i\gamma_R}{\sqrt{2}}, \quad (1.1)$$

where $\gamma_i = \gamma_i^\dagger$ are Majorana operators that satisfy $\{\gamma_i, \gamma_j\} = 2\delta_{ij}$.

In a sufficiently long nanowire, MBS are decoupled from each other, and noise sources will interact with each of them individually. The interaction with a single MBS is proportional to a single Majorana operator, i.e. $\gamma \sim f + f^\dagger$, and thus it will change the parity of the system. In a superconductor, however, electrons can only enter or leave as Cooper pairs, which means that the parity is conserved. Therefore, individual MBS are immune to local noise sources.

Consequently, only even powers of Majorana operators are allowed in the Hamiltonian. The simplest allowed term describes the coupling of a pair of MBS. In a single nanowire, or in a linear array of them, it is only possible implement this term with successive MBS. It is given by,

$$H_{pair} = iE_{LR}\gamma_L\gamma_R = E_{LR}(1 - 2f^\dagger f). \quad (1.2)$$

Here, E_{LR} is the tunnelling coupling between the two MBS. Consequently, a general state within the degenerate subspace evolves as,

$$|\Psi\rangle = \alpha|0\rangle + \beta|1\rangle \rightarrow U(t)|\Psi\rangle = \alpha|0\rangle + \beta e^{iE_{LR}t}|1\rangle. \quad (1.3)$$

However, universal quantum computation cannot be built from using only quadratic fermionic terms as in Eq. 1.2. Controlled interaction between MBS from different fermions

are essential to Majorana based quantum computation. Therefore, a higher dimensional structure where multiple MBS converge is required in order to do Majorana computation.

1.3. Experimental platforms

MBS can be realised in quasi one-dimensional systems defined on two-dimensional electron gases (2DEGs), or semiconducting nanowires, with strong spin-orbit and in proximity to a superconductor. The Hamiltonian that realises a Majorana nanowire is,

$$\mathcal{H} = \sum_k \Psi_k^\dagger H(k) \Psi_k, \quad H(k) = \left[\frac{|\mathbf{k}|^2}{2m^*} - \mu + \alpha(k_x \sigma_y - k_y \sigma_x) \right] \tau_z + B_x \sigma_x + \Delta \tau_x. \quad (1.4)$$

Here, $\Psi_k^\dagger = (f_{k\uparrow}^\dagger, f_{k\downarrow}^\dagger, f_{k\uparrow} f_{k\downarrow})^T$ are the Nambu spinors in k space, μ is the chemical potential, \mathbf{k} is the 2D wave-vector, α is the spin orbit interaction, B_x is the Zeeman field, Δ is the superconducting gap, and σ and τ are Pauli matrices for the spin and particle-hole basis. MBS appear as zero energy excitations of this Hamiltonian when $B_x^2 \geq \sqrt{\mu^2 + \Delta^2}$.

Realising such material combination is a challenge, and MBS transport signatures are not unambiguous. For example, superconductivity and magnetic fields compete with each other. On the other hand, MBS signatures can be reproduced by states localised in material defects or impurities. Consequently, most of the current work in this field is focused on unambiguously finding a single MBS pair.

Truly one-dimensional systems do not exist. There is a translational invariant direction, and at least one direction with finite width W . The energy of each mode has a contribution from both, and it is given by,

$$E_n(k) = \frac{\hbar^2}{2m^*} \left(k^2 + \frac{\pi^2 n^2}{W^2} \right). \quad (1.5)$$

Here, m^* is the effective mass and the spin orbit splitting is not considered. Independent MBS with different momentum profiles can be formed at each transverse mode when the chemical potential is at the bottom of the corresponding band.

1.3.1. Two dimensional electron gases

In order to build a multi Majorana device we require a flexible 2D platform where multiple nanowires can be easily attached. Furthermore, it been shown that properties of Majorana devices can be modulated by changing the device geometry *2DEGs appear as an interesting platform for since arbitrary geometries can be created using electrostatic gates.* On the other hand, high-quality networks of semiconducting nanowires can be built, but geometries are limited to straight configurations.

Parallel Majorana nanowires are the basic elements for a complex Majorana device. A single nanowire on a 2DEG can be created by adding a superconducting strip on top of the selected region as shown in Fig. . Then, a top gate is deposited next on top of the device such that depletes the surrounding 2DEG. A narrow quasi-one dimensional channel is created below the superconductor where the gate electric field is screened. Following this procedure, multiple parallel nanowires can be created in a 2DEG by selectively depositing superconducting covers.

There are several Majorana experiments on 2DEGs that have shown promising evidence for scalable and complex devices. Initial experiments[2, 4] focused on characterising the

properties of semiconducting layers with a superconducting cover. Advances in material growth allowed for clean interfaces with a hard superconducting gap to develop into the nanowire region. Later experiments focused on tunnel spectroscopy of stripe-like geometries[5] where a zero bias peak (ZBP) was found. However, due to disorder and defects such ZBPs have most likely a trivial origin from Andreev states rather than MBS. Nevertheless, efforts to develop complex devices in 2DEGs are made and new promising materials are being studied.

1.3.2. Electrostatic gates

The potential landscape in a 2DEG can be controlled by deposition of metallic gates on a top layer with an insulating barrier in between that smooths the potential profile. *The electrostatic potential in a 2DEG is found by solving the Poisson equation using a finite elements method on the device geometry.* The potential landscape, $U(\mathbf{r})$, for a given geometrical configuration can be found by solving Laplace equation,

$$\nabla \cdot [\epsilon_r(\mathbf{r}) \nabla U(\mathbf{r})] = 0. \quad (1.6)$$

Here, ϵ_r is the relative permittivity of each layer in the material stack. In general, the quantum electrostatics problem is more complicated due to the interaction of dopant charges with the potential. However, our problem is simpler since no extra charges are required.

1.4. Majorana bound states in a trijunction

In order to create a Majorana qubit, at least three MBS with local pair interactions are required. The device that realises this selective coupling is called a trijunction. It contains two parts: three nanowires, and a central cavity that mediates the coupling. In such a system, demonstration of the simplest non-trivial Majorana evolution experiment can be done.

The geometrical configuration of the trijunction is subject to two main constraints: On one hand, nanowires must be parallel since the topological phase closes for small deviations of the magnetic field. On the other hand, nanowires must have a significant separation from each other such that MBS are well isolated. Consequently, the design of a trijunction geometry with selective coupling between MBS pair is a non-trivial task.

Previous trijunction designs[1] have studied MBS coupling in the tunnelling regime. The trijunction is defined using gates placed on top of a 2DEG, and it is operated by controlling the voltages of the different gates. In this context, the MBS coupling relies entirely on wavefunction overlap along the cavity. Consequently, MBS pairs acquire relatively small couplings with the advantage of not introducing any extra sub gap state.

On the other hand, in the strong coupling the MBS coupling is mediated by cavity states but with extra levels present inside the gap. Nevertheless, the coupling energy of the MBS pairs can become significantly larger, i.e. comparable with the induced gap. The modulation of the coupling now relies on the cavity geometry. Interestingly, it has been shown that properties Majorana devices can be optimised by using geometrical effects. In this context, this work explores the geometrical dependence of selectively coupling multiple MBS pairs in a Majorana trijunction.

2

Trijunction of Majorana nanowires

In this chapter we demonstrate that the coupling of three pairs of MBS in a trijunction is determined by the geometrical details of the central semiconducting cavity. For certain geometrical configurations, a MBS pair couples resonantly with successive cavity states as in the so-called *resonant trapping*, while in other cases the coupling is mediated by individual non-overlapping levels.

We simulate the pair coupling of three Majorana nanowires mediated by a semiconducting cavity using Kwant. For each experiment, a pair of nanowires is set to host MBS in each sub band while the other nanowire is fully depleted. We consider the strong coupling regime where there are no tunnel barriers between the cavity and the nanowires. Furthermore, the phase difference between the selected nanowires is tuned such that the coupling is at a maximum. *The coupling energy of each pair is extracted as the value of the lowest non-zero eigenvalue with respect to the cavity chemical potential.*

The cavity chemical potential is varied in a range of 4 meV around the first resonance for all cavities. In this range, there are multiple levels that couple resonantly with a given pair of MBS. *In order to characterise the coupling, we extract the highest resonance peak for each geometry.* Then, we classify them according to their operational robustness, that is, height and width.

2.1. Quasi-one dimensional cavities

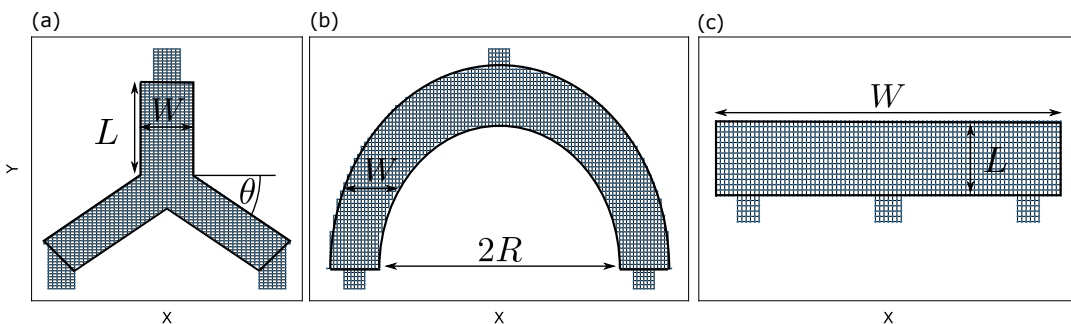


Figure 2.1: Kwant systems describing the three quasi-1D cavities: (a) Y-shaped defined by three parameters: arms length and width, L and W , and lateral arms angle θ . (b) Half-ring defined by the radius R and the width W . (c) Rectangular stripe defined by the length L and width W .

Let us start by building the simplest possible Majorana trijunction. Consider a quasi-1D cavity with mirror symmetry along the y -axis. Then, the position of the three nanowires is fixed: one is attached at the center, and one at each end. Consequently, the phase shift for the central MBS pairs is symmetric around π . Similarly, the coupling of the left-center MBS pair and center-right MBS pair is the same. Under these constraints, we study how the geometry affects the coupling of the two different pairs.

We consider three cavity geometries: In Fig. 2.1 (a) one can observe a Y-shaped cavity. In Fig. 2.1 (b) one can observe a half-ring stripe cavity with three nanowires attached in a fork-like geometry. In Fig. 2.1 (c) one can observe a rectangular stripe cavity with three Majorana nanowires attached.

It is a challenge to build a trijunction that reliably and selectively couples all three pairs of MBS. It is straightforward to couple a single MBS pair in a quasi-1D geometry since the left and right MBS pair will fully enclose the cavity wavefunctions. However, it is a challenge to create a system where the remaining two pairs can couple in a similar way.

2.1.1. Size dependence

Initially, the overall size of the system is varied, and a transition from the small to the long junction regime is found for all geometries. In Fig. 2.2 one can observe the evolution of the largest resonance peak for each geometry as a function of the system size.

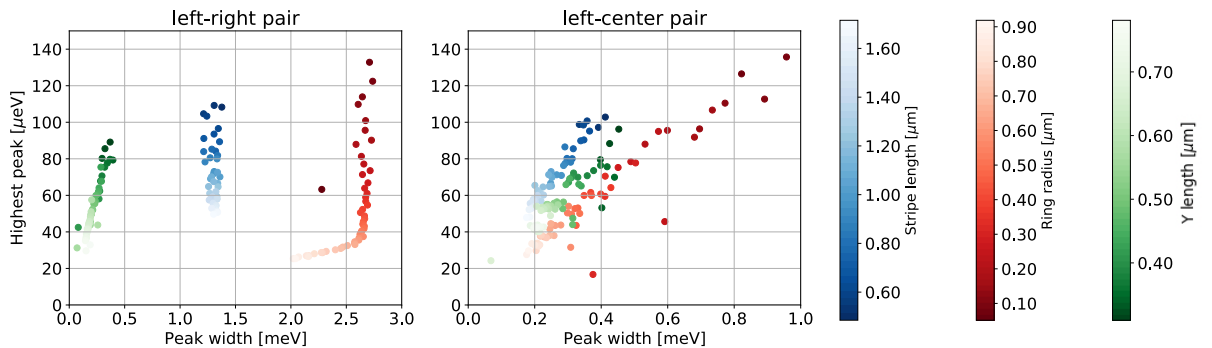


Figure 2.2: Geometrical dependence of the resonant coupling peaks for three quasi-1D geometries that correspond to each colorbar. The system was tuned to the lowest Majorana band. (a) Left-right MBS pair coupling. (b) Left-center MBS pair coupling.

The coupling of the left and right MBS pair shows a clear geometrical dependence as can be observed in Fig. 2.2 (a). Each geometry occupies a separate region in the resonant height-width plane. The ring cavity has the most robust resonant peaks. For small R , the coupling is larger than any other geometry, and it is close to $\Delta/2$. Similarly, the width is the largest, and it persists even for rings with diameter $1 \mu\text{m}$ after which decays. Then follows the stripe geometry that has approximately the same width for all considered widths. Finally, the Y-shaped cavity has overall the smallest resonant peak width.

The coupling of the central MBS pairs, on the contrary, cannot be easily separated for each geometry. Generally, one can see three diagonal stripes in Fig. 2.2 (b) where the stripe geometry has the largest resonant peak height. The peak width decreases as the size increases, and it has the same slope for all geometries. Nevertheless, for sufficiently small sizes, the ring geometry has peak heights and widths larger than any other geometry.

2.1.2. Resonant trapping

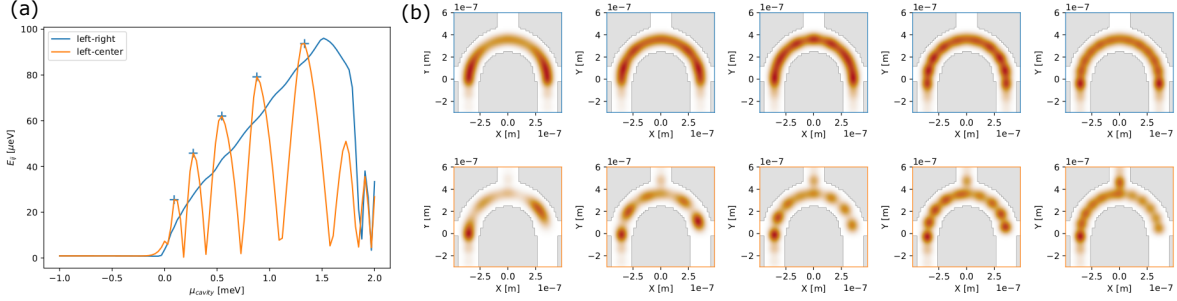


Figure 2.3: Spectra for a half-ring shaped cavity of width $W = 110$ [nm] and radius $R = 300$ [nm]. The system was tuned to the lowest Majorana band. (a) Coupling of each MBS pair. Center-right pair is the same curve as left-center pair. Crosses indicate the positions at where the wavefunction (b) are taken. The color of the frame in (b) corresponds each MBS pair in (a).

Let us consider the half-ring cavity. When the left and right nanowires are close to the ends of the cavity, the MBS pair couple along a sequence of overlapping resonant states as can be seen in the blue line of Fig. 2.3 (a). *The cavity states interfere constructively and the coupling accumulates creating a single wide peak over the resonant region.* It depends crucially on having the lead states around all of the cavity wavefunction as can be seen in Fig. 2.3 (b). This phenomena is known as *resonant trapping*.

For the central pairs coupling, in contrast, a band of resonances cannot form since the cavity wavefunction is not fully enclosed. When coupling the left and central MBS, the cavity region close to the right lead acts as a particle in a box with multiple individual levels that repel each other. Consequently, we observe the orange line shown in Fig. 2.3 (a) where the resonant band is divided in individual resonances.

The difference when coupling multiple MBS pairs relies on the geometric configuration of the cavity wavefunctions and the MBS relative positions. *Then, one can explain the distribution of couplings observed in Fig. 2.2.* The left and right MBS in the ring and stripe geometry have an approximately constant and large widths over the different system sizes because cavity levels remain resonant. On the other hand, the coupling of the central MBS pairs in any geometry has a much smaller width because some part of the wavefunction is not coupled. Particularly, the Y-shaped junction has a small width for all pairs because no resonant trajectories can be created in such geometry.

2.2. Two dimensional cavities

In a ballistic cavity, the motion of the electrons is determined by the shape of the cavity and leads. The electrons follow semiclassical trajectories connecting different leads that can be identified as peaks in the conductance. Following such intuition, we explore if changes in the geometry of a 2D cavity can be used to modulate the coupling of different MBS pairs. Particularly, we explore how the angular dependence of the incoming modes, and internal angles of the cavity, influence the MBS coupling.

We consider three geometries: In Fig. 2.4 (a) one can observe a circular cavity with Majorana nanowires attached in a fork-like geometry. In this geometry one can control the angle of the incoming MBS. In Fig. 2.4 (b) one can observe a triangular cavity with nanowires attached at the lower side. In this geometry one can control the angle of MBS

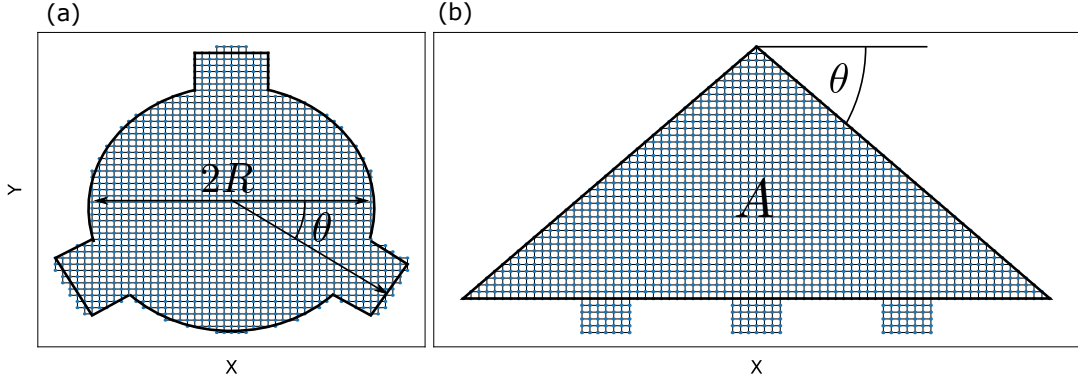


Figure 2.4: Left: Kwant system of a half-ring shaped cavity. It is defined by the radius R and the width W . Thinner rectangular segments represent the positions of the Majorana nanowires attached. Right: Lowest four eigenstates of the cavity with the nanowires fully depleted.

scattering within the cavity by changing the diagonal sides. In order to explore the role of the positioning of the leads, we explore a variation of the triangular geometry with the central lead in the top side. Lastly, we consider a rectangular geometry that can be created by extending the length of the stripe geometry shown in Fig. 2.1 (c).

2.2.1. Size dependence

Let us start by discussing the size dependence of the cavities. In Fig. 2.5 one can observe the size dependence of the resonant peak for the three two-dimensional geometries.

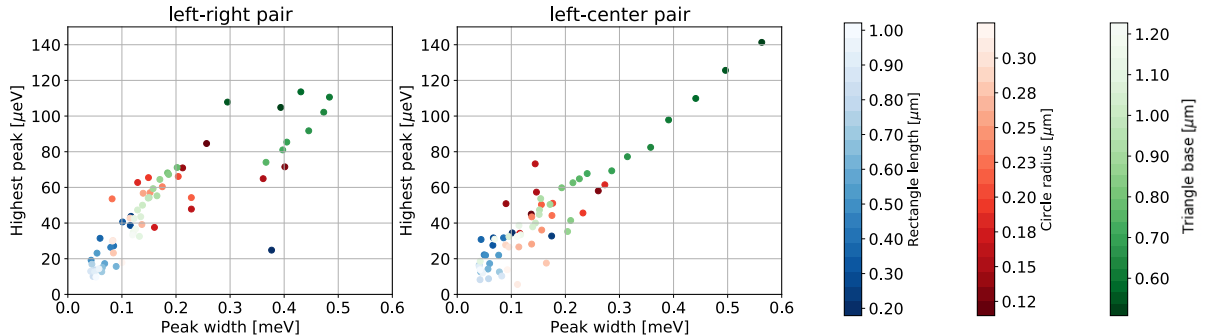


Figure 2.5: Size dependence of the three 2D geometries considered in this section corresponding to each colorbar. The system was tuned to the lowest Majorana band. The (a) left-right and (b) left-center largest resonant peaks are shown. The angle of all the cavities here is $\theta = \pi/4$.

Overall, there is no major distinction between the coupling of different pairs. All couplings decay as the system size increases following a diagonal line in panels (a) and (b). Nevertheless, the geometry dependence can be seen in three different regions along the diagonal.

On the rightmost region, one observes that the triangular geometry has the largest couplings and widths for small sizes. Descending along the diagonal, the triangular and circular geometries overlap. Remarkably, there is a significant size difference between them in the overlapping region, approximately 500 nm. Most of circular geometries are concentrated in this region. At the bottom of the diagonal, one observes that the worst MBS couplings happen for rectangular geometries.

2.2.2. Angular dependence

The angle is changed in two triangular cavities, one circular cavity, and the Y-shaped cavity. The resulting coupling for each pair and geometry is shown in Fig. 2.6.

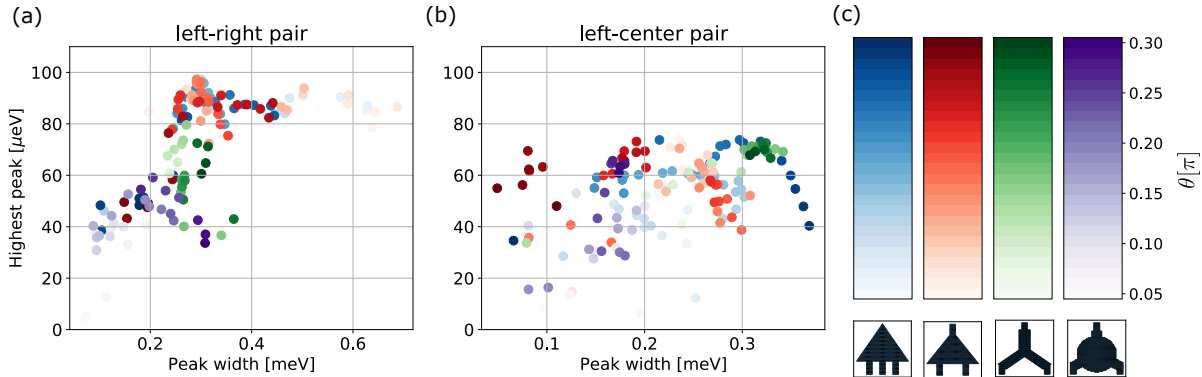


Figure 2.6: Angular dependence of the resonant coupling peaks for four geometries with angle dependence. The system was tuned to the lowest Majorana band. Each one corresponds to a colorbar as depicted in (c). (a) Left-right MBS pair coupling. (b) Left-center MBS pair coupling. The area of the triangular cavities was $A = 900 [a^2]$. The radius of the circular cavity is $R = 250 [\text{nm}]$. The size of the Y-shaped cavity is similar to that of the triangular cavity.

The triangular geometry shows a transition from the resonant trapping regime to the single resonance regime while maintaining an approximately constant peak height. One can observe that the peak height stays around the same value for a large range of angles in panel (a). This behaviour is present in both triangular geometries since the red and blue dots highly overlap. The width, on the other hand, is inversely proportional to the angle. For small angles, the width is the largest for 2D geometries, around 0.7 meV. As the angle increase, the width decreases until it saturates around 0.3 meV.

In order to understand this behaviour, let us observe that for small angles the triangular cavity resembles a quasi-1D system. By cutting the edges of the stripe geometry, the wavefunction is concentrated towards the center such that it can be easily trapped between the left and right leads as observed in the blue curve of Fig. 2.7 (a). As the angle increases, the resonant band splits into several sub bands that contain a few resonances each as observed in Fig. 2.7 (b). If the angle increases further, these resonances fully split into individual levels, thus explaining the saturation found in Fig. 2.6 (a).

The coupling of the left and central MBS pair -on the contrary- is more complicated to analyse due to the high overlap between geometries as observed in Fig. 2.6 (b). Couplings for both triangular geometries are around the same region in width and height for small angles. As the angle increases, the width of the configuration with central lead at the lower side (blue) increases, while the other configuration (red) decreases.

It is remarkable that the triangular geometry has two configurations that can be used to operate a Majorana trijunction with similar coupling magnitude and width for all MBS pairs. These two configurations are shown in Fig. 2.7. Note, however, that the small angle configuration would be rather considered a quasi-1D system since the ration between its dimensions. That is the reason why the resonant band has such a large width and encloses many states. Nevertheless, resonant trapping is still present in the second configuration, but with fewer states inside the resonant band.

For the remaining geometries, there is indeed a modulation for the left and right MBS

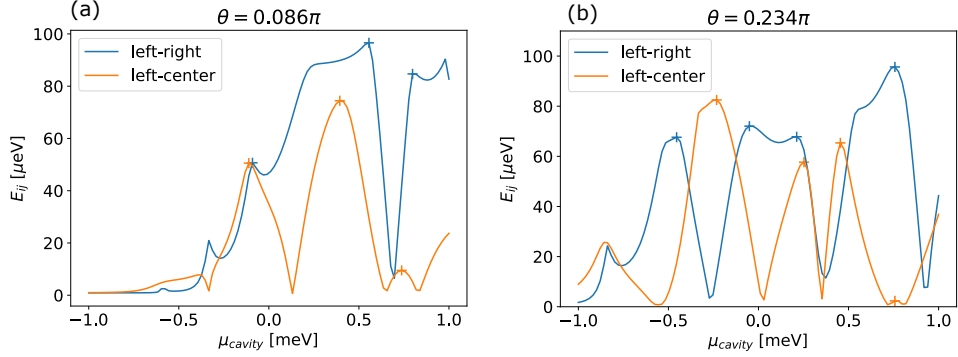


Figure 2.7: Coupling of triangular geometries with the central lead at the (a) top and (b) bottom sides. The total area of the triangle is $A = 1200 [\text{a}^2]$.

pairs. However, the overall coupling remains smaller and narrower than the triangular case. Interestingly, the left and central MBS coupling for the Y-shaped cavity converges to a region around $(0.3\text{meV}, 70\mu\text{eV})$ as the angle increases (see Fig. 2.6 (b) green points). On the other hand, the behaviour of this pair in the circular cavity does not show a clear trend.

2.2.3. Majorana sub bands

By tuning each nanowire sub band into the topological phase, we probe the momentum distribution of the cavity states. In Fig. 2.8 one can observe the mean coupling for each band. It has been averaged over all geometrical configurations and all MBS pairs since no clear distinction between them was found.

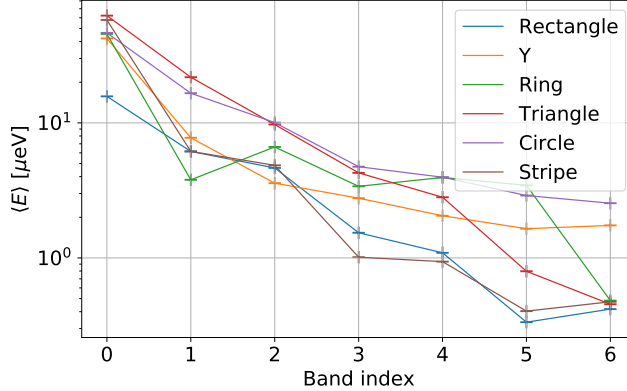


Figure 2.8: Mean geometry-pair coupling for all Majorana sub band and all geometries considered in this section. The geometry average was taken over the data shown in Fig. 2.5.

Overall, the coupling decays exponentially as the band index increases. The decay is modulated by the geometry, but the trend holds in all cases. There is, approximately, two order of magnitude decrease in the coupling from the lowest to the highest band.

The lowest band carries the largest coupling. This allows us to infer that the momentum distribution of cavity states is dominated by low momentum states. This is reasonable since the coupling of spatially separated MBS requires delocalised cavity states. However, a precise quantitative description of the momentum profiles inside the cavity goes beyond the scope of this work.

3

Gate defined triangular cavities

In the previous chapter we have found that the best geometries to couple MBS are the ring and the triangular geometries. The coupling of different pairs is highly asymmetric in the ring geometry, while it is similar in the triangular geometry. Then, we consider that a triangular trijunction is more reliable when selectively coupling multiple MBS pairs.

In this chapter, we simulate a gate defined triangular cavity and describe how it can be used as a switch coupling different MBS pairs. The electrostatic potential is found as the solution to Eq. (??) using the finite element solver from Ref. . In practice, the cavity region in the trijunction is filled with the electrostatic potential, while the nanowires are set to a step like-potential.

3.1. Gates configuration

A trijunction is a complex Majorana device that can be implemented on a 2DEG by selectively depositing electrostatic gates. It contains two main regions: three nanowires and a semiconducting cavity. We focus on the design of a gate defined triangular cavity. We do not consider the electrostatic modeling of the nanowires since one can assume that the electric field in the nanowires is screened by the superconductor.

The gates are placed in a single layer above the 2DEG with a dielectric layer in the middle as shown in Fig. . Different layer configurations were explored, and a single layer was found to be the best in terms of shape-resolution and voltage range. The thickness of each layer determines how much the electric field penetrates into the 2DEG. We consider typical parameters from experiments as described in the inset of Fig. .

Let us consider the two gate configurations shown in Fig. for the cavity region. There are three kinds of gates:

1. Plunger gate: Defines and controls the potential inside the triangular cavity region.
2. Screen gates: There are two kinds of screen gates: First, the triangular screen gates deplete the 2DEG around the plunger gate, which contributes to the overall triangular shape. Second, the screen barrier gates between the tunnel gates that keep each nanowire channel separated from the others.
3. Barrier gates: Modulate the coupling between each nanowire and the cavity. They allow to tune the system in the insulating, tunnelling, and strong coupling regimes.

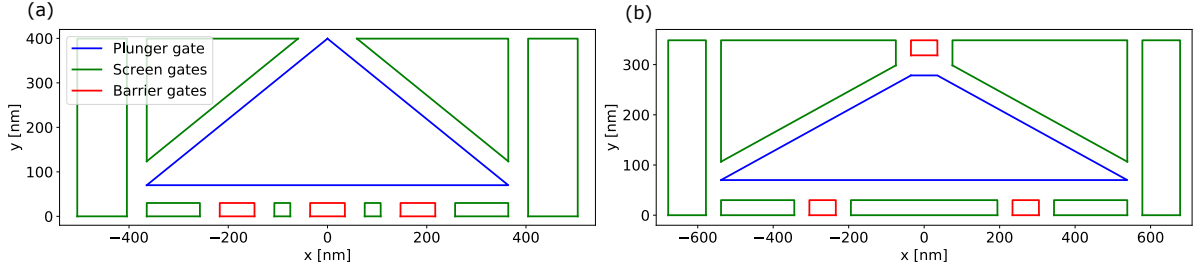


Figure 3.1: Gate configuration of the two triangular cavities considered. The area is set $A = 1200 [a^2]$. (a) Triangular cavity with angle $\theta = 0.234\pi$ with all nanowires at the lower side. (b) Triangular cavity with angle $\theta = 0.125\pi$ with central nanowire at the top side. Spacing between gates is set to 40 nm. Barrier gates have length 30 nm and width 70 nm. Nanowires (not shown) are attached at the ends of the barrier gates.

In general terms, to operate the device optimally we require the minimum number of tunable gates while having enough flexibility to connect different MBS pairs. There are three basic requirements that must be satisfied at all times:

1. Selectively couple different pairs of MBS via control of barrier gates.
2. Use the triangular screen gates to deplete the area surrounding the plunger gate.
3. There is always a barrier between successive tunnel gates by tuning screen barriers.

The first two requirements require us to calibrate the device with focus on varying the minimum number of gate voltages. The last requirement can be satisfied by choosing a sufficiently large screen barrier.

3.2. Device 1

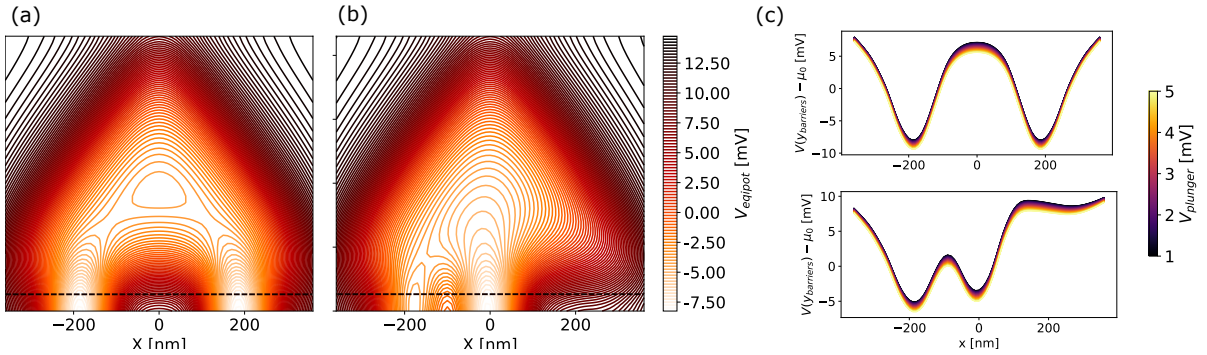


Figure 3.2: Equipotential lines inside the device for representative parameters of the (a) left and right MBS pair and (b) left and center MBS pair. Colorbar indicates value of equipotential lines. (c) Cut of the potential along the tunnel barriers, i.e. dashed black lines in (a) and (b), taken for a range of plunger gate voltages. Colorbar in (c) indicates the plunger gate voltage.

In this section we describe the operation of the gate configuration shown in Fig. 3.1 (a). In Fig. 3.3 (a) - (b) one can observe the potential inside the 2DEG for the coupling of each pair. In contrast to the geometrical model discussed in the previous chapter, the trijunction is defined in a smooth potential landscape. Therefore, it is not clear if the geometrical dependence that we discussed in Fig. ?? will hold.

3.2.1. Nanowire channels

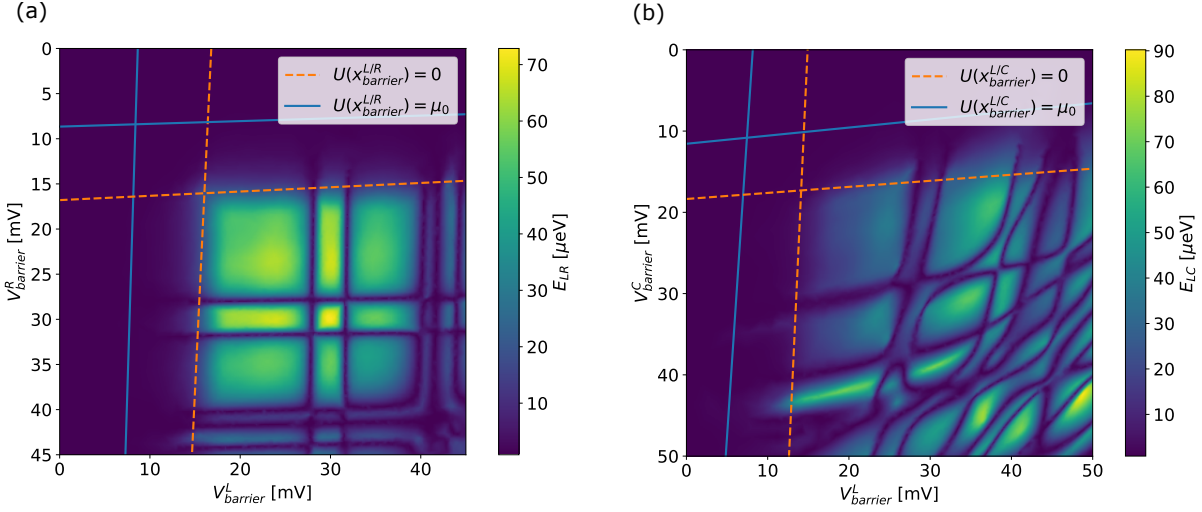


Figure 3.3: Coupling of (a) left and right MBS pair and (b) left and central MBS pair as a function of the corresponding barrier gates. Plunger gate is tuned around the first resonance. Gate voltages used correspond to those described in Table 3.2.

Operating the left and right tunnel barriers is straightforward since they are far from each other. Consequently, there is no interdependence between them as can be observed in Fig. 3.3 (a). On the other hand, the operation of the central pairs is not symmetric given the mutual influence of successive barrier gates. In Fig. 3.3 (b) one can observe that the slope of the potential crossings is not zero indicating cross interaction.

The system can be tuned in the insulating, tunnel, and strong coupling regimes by manipulating the barrier gates. The blue and orange lines in Fig. indicate the value of the potential at the bottom of the barrier gates with respect to μ_0 and 0, respectively. The tunnelling regime starts at the blue line, when the barrier potential crosses μ_0 . In this regime, the coupling is mediated by direct overlap of the MBS wavefunctions. Therefore, one observes a difference in the tunnelling regime of panels (a) and (b) since in the later the MBS are closer. The orange lines indicate the start of the strong coupling regime, after which the MBS coupling saturates.

As the barrier potential becomes more positive, there are two new effects: New crossings caused by resonant cavity levels appear. On the other hand, for very large barrier gates the screen barrier between them lowers and allows for direct coupling. The former can be seen clearly in panel (a) as the two crossings in the strong coupling regime. The latter can be seen in the lower right part of panel (b) where the coupling increases due to direct coupling. Nevertheless, keeping the barrier potential as small as possible makes these effects negligible.

3.2.2. Background potential

In contrast to the purely geometrical model, the triangular cavity can be deformed by tuning the screen gates, and new coupling regimes can be explored. By increasing the voltage of the screen gates, one confines the electronic density within the triangular cavity.

In Fig. 3.4 one can observe the MBS coupling as a function of the voltages of the two triangular screen gates for each pair. In panel (a) one observes that the case of the left

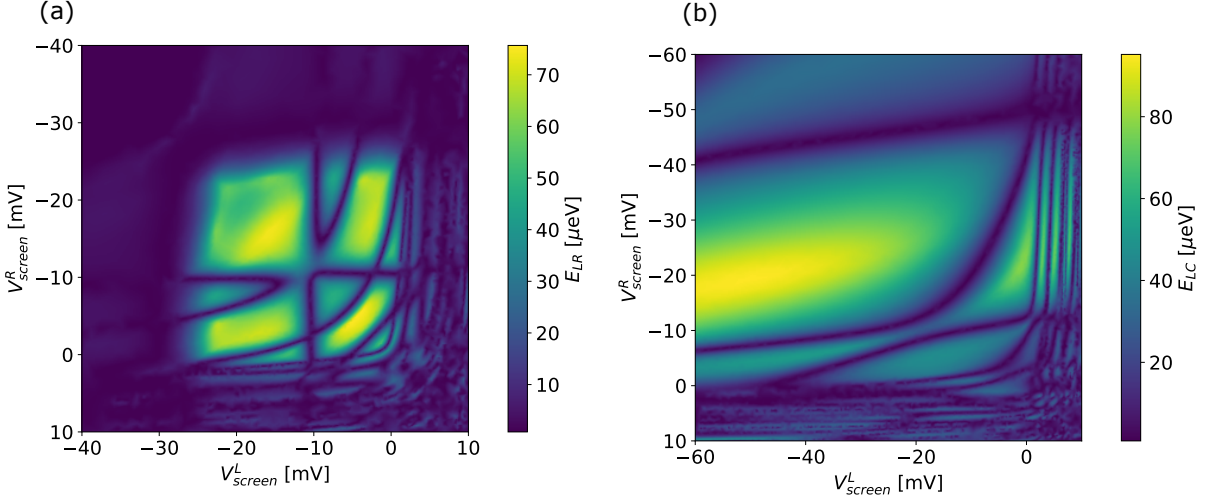


Figure 3.4: Coupling of (a) left and right MBS pair and (b) left and central MBS pair as a function of the triangular screen gates. Plunger gate is tuned around the first resonance. Gate voltages used correspond to those described in Table 3.2.

and right MBS pair is symmetric. As expected, there is a peak in the coupling when the electronic density is confined to the triangular cavity.

On the other hand, panel (b) shows a new regime for the coupling of the central MBS pairs. One observes that the coupling of the left central pair increases by increasing the potential in the right triangular screen gate. Effectively, the cavity becomes smaller, and the coupling increases due to a higher wavefunction overlap.

3.2.3. Device operation

The device is operated as a switch that maximises the coupling between different MBS pairs. Once a given pair is coupled, four gates are required to change in order to couple a different pair. Based on the discussion from the previous sections, the set of gate voltages that define the operational point of the device are shown in Table 3.2. One can observe that

	$V_{plunger}$	$V_{barrier}^L$	$V_{barrier}^R$	$V_{barrier}^C$	V_{screen}^L	V_{screen}^R
left-right	3	35	35	-20	-15	-15
left-center	1	35	-20	20	-15	40
center-right	1	-20	35	20	40	-15

Table 3.1: Gate voltage configuration used for coupling different MBS pairs. Voltage units are meV. Remaining gate voltages are fixed: screen barriers between nanowires -30 meV, screen barriers around nanowires -15 meV.

3.3. Device 2

In this section we describe the operation of the gate configuration shown in Fig. 3.1 (b). In Fig. 3.6 (a) - (b) one can observe the potential inside the 2DEG for the coupling of each pair. While the area in both devices is the same, this device has a smaller angle. The overall shape resembles a quasi-one dimensional system where resonant trapping is expected.

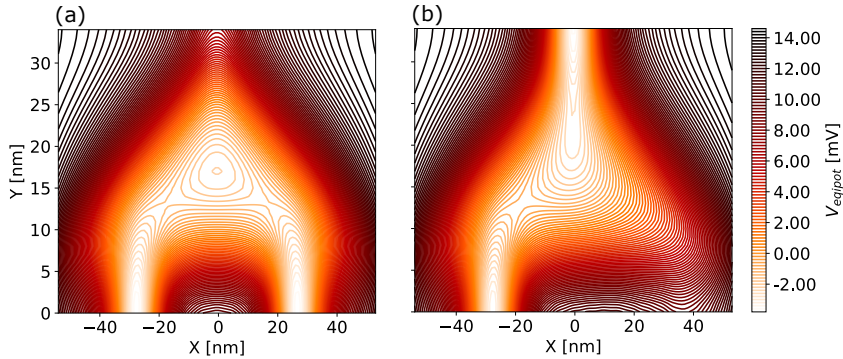


Figure 3.5: Equipotential lines inside the device for representative parameters of the (a) left and right MBS pair and (b) left and center MBS pair. Colorbar indicates value of equipotential lines. (c) Cut of the potential along the tunnel barriers, i.e. dashed black lines in (a) and (b), taken for a range of plunger gate voltages. Colorbar in (c) indicates the plunger gate voltage.

3.3.1. Nanowire channels

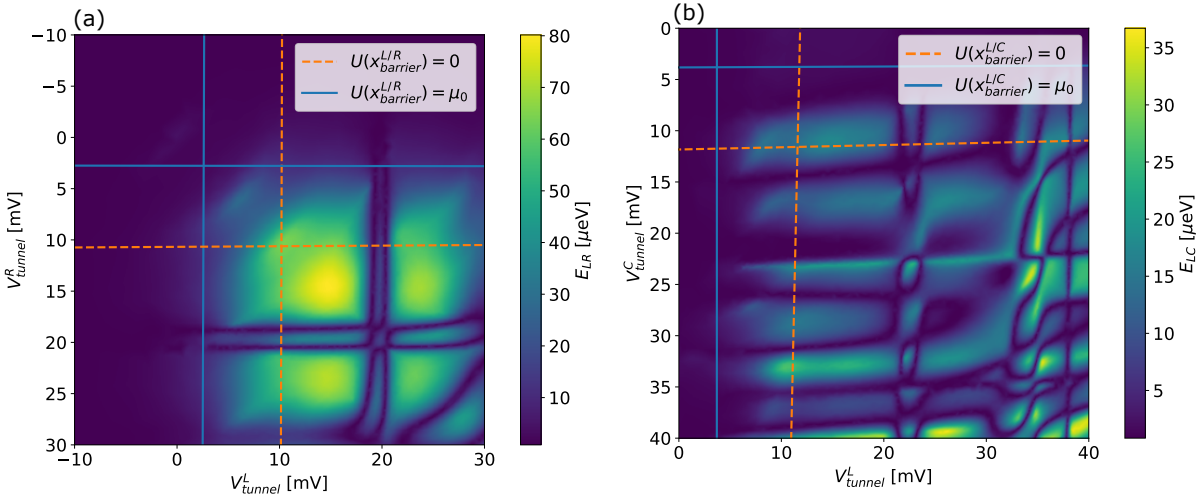


Figure 3.6: Coupling of (a) left and right MBS pair and (b) left and central MBS pair as a function of the corresponding barrier gates. Plunger gate is tuned around the first resonance. Gate voltages used correspond to those described in Table 3.2.

In contrast to the previous device, all barrier gates remain well separated from each other. Therefore, in Fig. 3.6 one observes that there is no interdependence of barrier gates. However, the system behaves effectively as a quasi-one dimensional cavity. Consequently, the coupling in the tunnelling regime is larger due to an increase in the wavefunction overlap.

In the strong coupling regime there is a large difference between the coupling of the different pairs. One can observe that panel (a) is similar to the previous case. On the other hand, panel (b) shows a very different behaviour that reflects the new structure of the cavity. This effect was not present in the purely geometric model, which suggest that it does not hold for gate defined cavities.

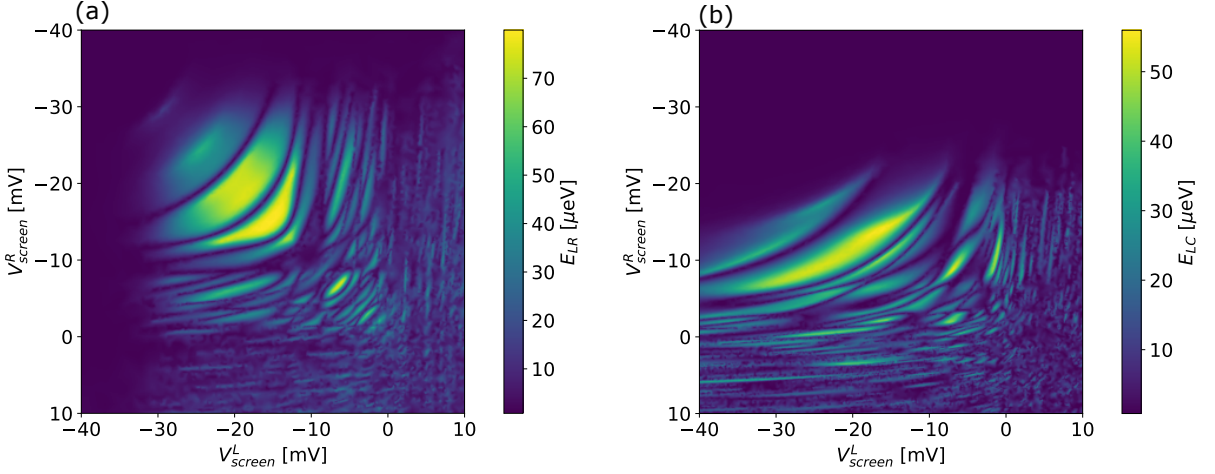


Figure 3.7: Coupling of (a) left and right MBS pair and (b) left and central MBS pair as a function of the triangular screen gates. Plunger gate is tuned around the first resonance. Gate voltages used correspond to those described in Table 3.2.

3.3.2. Potential background

In this device the position of the barrier gates is highly dependent on the surrounding screen gates as can be observed in Fig. 3.6. Therefore, it is not possible to strongly deform triangular cavity without disconnecting the nanowires.

Similar as before, in Fig. 3.8 (a) one observes that there is a region where the MBS coupling for the left and right MBS pair has a maximum. This region corresponds to the electronic density concentrated under the plunger gate. Interestingly, the magnitude of the coupling is similar to the previous device.

The coupling of the central pairs as a function of the screen gates can be observed in panel (b). One can observe that there's a region where a maximum develops, but it remains smaller than the coupling of the left and right MBS pair. Furthermore, the coupling vanishes if the right triangular screen gate becomes very negative. This indicates that the barrier gate has been displaced from its position, and the central nanowire disconnects from the cavity.

If the screen gates are not tuned correctly, the coupling vanishes. If the screen gates are too negative, the area under the plunger gate is depleted, and the MBS cannot couple. Similarly, if is not negative enough, the electron density is extended over a rectangular region and the coupling becomes very small.

3.3.3. Device operation

This device can be used as a switch to couple different MBS pairs selectively. However, the magnitude of the coupling is highly asymmetric between pairs. Consequently,

3.4. Devices comparison

	$V_{plunger}$	$V_{barrier}^L$	$V_{barrier}^R$	$V_{barrier}^C$	V_{screen}^L	V_{screen}^R
left-right	6	17	17	-20	-15	-15
left-center	6.7	17	-20	17	-10	-20
center-right	6.7	-20	17	17	-20	-10

Table 3.2: Gate voltage configuration used for coupling different MBS pairs. Voltage units are *meV*. Remaining gate voltages are fixed: screen barriers between nanowires -30 meV, screen barriers around nanowires -15 meV.

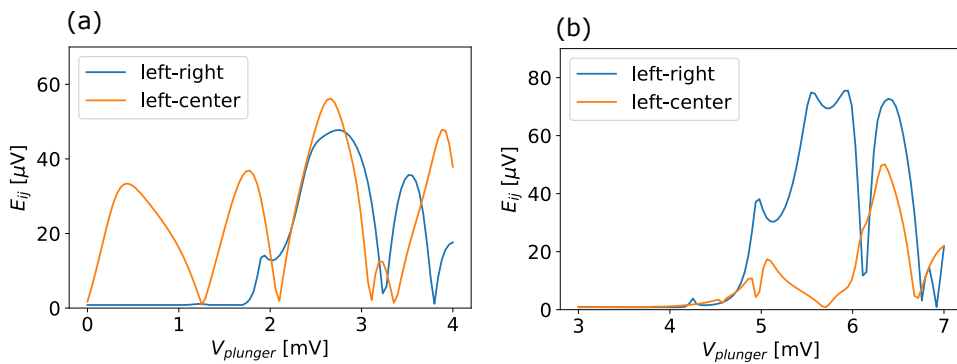


Figure 3.8

4

Conclusions

1. Triangular cavities show a maximum coupling for a certain angle for the far pair, while the coupling of the central pair can be tuned to a maximum or minimum depending on the wire's side.
2. In a gate defined cavity, the position of the nanowires plays a crucial role in the definition and tunability of the triangular shape and thus enhancing or decreasing the MBS coupling.
3. A natural extension of this work is to design an experiment where joint parity measurements can be measured via interferometry in a loop geometry, or via charge measurements with a nearby sensor.
4. Another possible extension is to include realistic noise, representing the etching process, as potential irregularities along the triangle sides.
5. In conclusion, a trijunction of MBS where the coupling of all pairs is comparable to the superconducting gap has been designed and the operation of the device has been discussed in terms of electrostatic gates.

Bibliography

- [1] M. Hell, J. Danon, K. Flensberg, and M. Leijnse. Time scales for majorana manipulation using coulomb blockade in gate-controlled superconducting nanowires. *Physical Review B*, 94:1–32, 2016.
- [2] M. Kjaergaard, F. Nichele, H. J. Suominen, M. P. Nowak, M. Wimmer, A. R. Akhmerov, J. A. Folk, K. Flensberg, J. Shabani, C. J. Palmstrom, and C. M. Marcus. Quantized conductance doubling and hard gap in a two-dimensional semiconductor-superconductor heterostructure. 3 2016.
- [3] C. M. Moehle, C. T. Ke, Q. Wang, C. Thomas, D. Xiao, S. Karwal, M. Lodari, V. van de Kerkhof, R. Termaat, G. C. Gardner, G. Scappucci, M. J. Manfra, and S. Goswami. Insbas two-dimensional electron gases as a platform for topological superconductivity. 5 2021.
- [4] J. Shabani, M. Kjaergaard, H. J. Suominen, Y. Kim, F. Nichele, K. Pakrouski, T. Stankevic, R. M. Lutchyn, P. Krogstrup, R. Feidenhans'l, S. Kraemer, C. Nayak, M. Troyer, C. M. Marcus, and C. J. Palmstrøm. Two-dimensional epitaxial superconductor-semiconductor heterostructures: A platform for topological superconducting networks. 11 2015.
- [5] H. J. Suominen, M. Kjaergaard, A. R. Hamilton, J. Shabani, C. J. Palmstrøm, C. M. Marcus, and F. Nichele. Zero-energy modes from coalescing andreev states in a two-dimensional semiconductor-superconductor hybrid platform. 3 2017.